Journal of Sedimentary Research

How distinctive are flood-triggered turbidity currents?

--Manuscript Draft--

Manuscript Number:	2020-168R2
Article Type:	Current Ripples
Corresponding Author:	Catharina Heerema Durham University Durham, Durham UNITED KINGDOM
First Author:	Catharina J. Heerema
Order of Authors:	Catharina J. Heerema
	Matthieu J.B. Cartigny
	Ricardo Silva Jacinto
	Stephen M. Simmons
	Ronan Apprioual
	Peter J. Talling
Abstract:	Turbidity currents triggered at river mouths form an important highway for sediment, organic carbon, and nutrients to the deep sea. Consequently, it has been proposed that the deposits of these flood-triggered turbidity currents provide important long-term records of past river floods, continental erosion, and climate. Various depositional models have been suggested to identify river-flood-triggered turbidite deposits, which are largely based on the assumption that a characteristic velocity structure of the flood-triggered turbidity current is preserved as a recognizable vertical grain size trend in their deposits. Four criteria have been proposed for the velocity structure of flood-triggered turbidity currents: prolonged flow duration; a gradual increase in velocity; cyclicity of velocity magnitude; and a low peak velocity. However, very few direct observations of flood-triggered turbidity currents exist to test these proposed velocity structures. Here we present direct measurements from the Var Canyon, offshore Nice in the Mediterranean Sea. An acoustic Doppler current profiler was located 6 km offshore from the river mouth, and provided detailed velocity measurements that can be directly linked to the state of the river. Another mooring, positioned 16 km offshore, showed how this velocity structure evolved down-canyon. Three turbidity currents were measured at these moorings, two of which are associated with river floods. The third event was not linked to a river flood and was most likely triggered by a seabed slope failure. The multi-pulsed and prolonged velocity structure of all three (flood and landslide triggered) events is similar at the first mooring, suggesting that it may not be diagnostic of flood triggering. Indeed, the event that was most likely triggered by a slope failure matched the four flood-triggered criteria best, as it had prolonged duration, cyclicity, low velocity, and a gradual onset. Hence, previously assumed velocity-structure criteria used to identify flood-triggered turbidity currents may be produced by other triggers. Next, this study shows how the proximal multi-pulsed velocity structure reorganizes down-canyon to produce a single velocity pulse. Such rapid-onset, single-pulse velocity structure has previously been linked to landslide-triggered events. Flows recorded in this study show amalgamation of multiple velocity pulses leading to shredding of the flood signal, so that the original initiation mechanism is no longer discernible at just 16 km from the river mouth. Recognizing flood-triggered turbidity currents and their deposits may thus be challenging, as similar velocity structures can be formed by different triggers, and this proximal velocity structure can rapidly be lost due to self-organization of the turbidity current.

How distinctive are flood-triggered turbidity currents?

Catharina J. Heerema[1], Matthieu J.B. Cartigny[1], Ricardo Silva Jacinto[2], Stephen M. Simmons[3], Ronan Apprioual[2], Peter J. Talling[1]

[1]Departments of Earth Science and Geography, Durham University, Lower Mountjoy, South Rd, Durham DH1 3LE, United Kingdom

[2]IFREMER, Géosciences Marines, Centre de Bretagne ZI Pointe du diable CS 10070, 29280 Plouzané, France

[3] Energy and Environment Institute, University of Hull, Hull HU6 7RX, United Kingdom

ABSTRACT

Turbidity currents triggered at river mouths form an important highway for sediment, organic carbon, and nutrients to the deep sea. Consequently, it has been proposed that the deposits of these flood-triggered turbidity currents provide important long-term records of past river floods, continental erosion, and climate. Various depositional models have been suggested to identify river-flood-triggered turbidite deposits, which are largely based on the assumption that a characteristic velocity structure of the flood-triggered turbidity current is preserved as a recognizable vertical grain size trend in their deposits. Four criteria have been proposed for the velocity structure of flood-triggered turbidity currents: prolonged flow duration; a gradual increase in velocity; cyclicity of velocity magnitude; and a low peak velocity. However, very few direct observations of flood-triggered turbidity currents exist to test these proposed velocity structures. Here we present direct measurements from the Var Canyon, offshore Nice in the Mediterranean Sea. An acoustic Doppler current profiler was located 6 km offshore from the river mouth, and provided detailed velocity measurements that can be directly linked to the state of the river. Another mooring, positioned 16 km offshore, showed how this velocity structure evolved down-canyon. Three turbidity currents were measured at these moorings, two of which are associated with river floods. The third event was not

linked to a river flood and was most likely triggered by a seabed slope failure. The multi-pulsed and prolonged velocity structure of all three (flood and landslide triggered) events is similar at the first mooring, suggesting that it may not be diagnostic of flood triggering. Indeed, the event that was most likely triggered by a slope failure matched the four flood-triggered criteria best, as it had prolonged duration, cyclicity, low velocity, and a gradual onset. Hence, previously assumed velocity-structure criteria used to identify flood-triggered turbidity currents may be produced by other triggers. Next, this study shows how the proximal multi-pulsed velocity structure reorganizes down-canyon to produce a single velocity pulse. Such rapid-onset, single-pulse velocity structure has previously been linked to landslide-triggered events. Flows recorded in this study show amalgamation of multiple velocity pulses leading to shredding of the flood signal, so that the original initiation mechanism is no longer discernible at just 16 km from the river mouth. Recognizing flood-triggered turbidity currents and their deposits may thus be challenging, as similar velocity structures can be formed by different triggers, and this proximal velocity structure can rapidly be lost due to self-organization of the turbidity current.

INTRODUCTION

Rivers directly connected to submarine channels and canyons are highly efficient in transporting large amounts of sediment, organic carbon, and pollutants to the deep sea (Galy et al., 2007). Consequently, the deep-sea depositional records from what have been interpreted as flood-triggered turbidity currents have been used to reconstruct paleo-floods (e.g., St-Onge et al., 2004; Plink-Björklund and Steel, 2004; see review by Zavala et al. (2011) and references therein) and their recurrence rates (Mulder et al., 2001; Nakajima, 2006). Such paleo-flood reconstructions rely on the underpinning assumptions that river floods create turbidity currents with a distinct velocity structure, and that this distinct velocity structure is recorded in the turbidite deposits through unique vertical grain size variations (Kneller and McCaffrey, 2003; Mulder et al., 2003). It is assumed that this vertical grain size trend translates to an identifiable velocity time series at a fixed point, from here on referred to as velocity structure. Proposed criteria to identify the velocity structure of a flood-triggered turbidity

current include: 1) a prolonged duration due to the long time scale of river flooding in comparison to most slope failures (Mulder et al., 2003; Zavala and Pan, 2018); 2) a gradual velocity increase at the start of the turbidity current (waxing) associated with the rising limb of the river discharge, followed by a waning turbidity current (Mulder et al., 2003); 3) multiple cycles of acceleration and deceleration (pulses) reflecting discharge fluctuations that are common in river floods (Khripounoff et al., 2012; Zavala and Pan, 2018); and 4) a low peak velocity, as flood-triggered turbidity currents are expected to be dilute and thus slow in comparison to the much denser landslide-triggered flows (Mulder et al., 2003; Nakajima, 2006; Khripounoff et al., 2012; Zavala and Pan, 2018). These four criteria are important in paleo-flood reconstructions as they are used to distinguish between flood-triggered and landslide-triggered turbidity currents, with landslide-triggered flows characterized by a sudden onset with a high peak frontal velocity (Kirwan et al., 1986; Normark and Piper, 1991; Kneller and Buckee, 2000; Mulder et al., 2003). However, there are few field observations of velocity structures in turbidity currents measured offshore from river mouths to validate such an approach. To our knowledge, there are just five locations with direct measurements of such velocity structures (Khripounoff et al., 2009, 2012; Liu et al., 2012; Hughes Clarke, 2016; Lintern et al., 2016; ; Azpiroz-Zabala et al., 2017; Hage et al., 2019; Simmons et al., 2020).

The velocity structures measured at these five locations of flood-triggered turbidity currents are not always consistent with the above-mentioned criteria. For example, observations in the Var Canyon, in the Mediterranean Sea, have shown that landslide-triggered events can last twice as long as flood-triggered events (Khripounoff et al., 2012). Events in the Congo Canyon have been measured to last up to 10 days (Simmons et al., 2020), although the events in the Congo Canyon are typically associated with elevated river discharge, and not flood peaks (Bailey et al., 2021). A gradual increase in velocity was measured in a flood-triggered turbidity current in the Gaoping Canyon, offshore Taiwan (Liu et al., 2012), but not in the flood-triggered flows in the Var Canyon (Khripounoff et al., 2012), on the Fraser Delta, British Columbia (Lintern et al., 2016), or at the Squamish Delta, British Columbia (Hughes Clarke, 2016; Hage et al., 2019). Although multiple cycles of acceleration and deceleration are observed in the Var Canyon (Khripounoff et al., 2012), they have not been observed

in the other locations (Liu et al, 2012, Lintern et al. 2016, Hughes Clarke, 2016; Hage et al. 2019). Finally, the Var Canyon observations show that flood-triggered flows are indeed somewhat slower than landslide-triggered flows (Khripounoff et al. 2012), but in the Gaoping Canyon the observations show opposite velocity trends, as turbidity currents linked to river floods are the fastest (Gavey et al., 2017). Moreover, the turbidity currents observed in some river-associated systems strongly resemble landslide-triggered flows with a single pulse characterized by a sudden onset (Hughes Clarke, 2016; Lintern et al., 2016; Azpiroz-Zabala et al., 2017; Hage et al., 2019; Simmons et al., 2020). Overall, the variability in the direct observations show that using the velocity structure of a turbidity current to identify a flood trigger is problematic and more field measurements are needed to understand these variations.

Several mechanisms could explain the inconsistencies observed in the velocity structures of flood-triggered turbidity currents. For example, the duration of a turbidity current can change significantly down canyon due to stretching of the flow (Azpiroz-Zabala et al., 2017). Initially slow flows can accelerate rapidly as they start to bulk up due to erosion of the seafloor (Parker et al., 1986; Sequeiros et al., 2009; Hage et al., 2019; Heerema et al., 2020), and multiple velocity pulses in the same event can merge, i.e., amalgamate (Kneller and McCaffrey, 2003; Ho et al., 2018). Additionally, the velocity structure of flood-triggered turbidity currents is likely to vary significantly depending on the exact process by which the sediment is transferred from the river to the turbidity current. Three such transfer mechanisms have been proposed for marine settings. First, at sufficiently high sediment concentrations (36-43 kg m^{-3}), excess sediment density causes a river plume to be denser than seawater, leading to a hyperpycnal river that plunges and continues along the seabed as a turbidity current (Mulder and Syvitski, 1995). Second, sea-surface (hypopycnal) river plumes can generate turbidity currents. Convective fingers of settling sediment can occur in such hypopycnal plumes at sediment concentrations of as little as 1 kg m^{-3} (Parsons et al., 2001). Third, substantially more dilute river plumes (0.07 kg m^{-3}) have recently been found capable of initiating turbidity currents, by generating high sediment concentration due to near-bed flow convergence in tidal settings (Hage et al., 2019). The range of possibilities outlined above, combined with the scarcity of seafloor

observations, severely limits paleo-flood reconstructions. High-resolution velocity measurements near the river mouth are needed to test the variability of turbidity currents close to the river mouth. Additionally, further velocity measurements down-canyon are needed to test how far down the system any potential flood-triggered velocity structure is preserved.

AIMS

Here we present new field measurements of three turbidity currents offshore from the Var River mouth. This study extends the earlier work of Khripounoff et al. (2009; 2012) in this system. In this new study, high-resolution acoustic Doppler current profiler (ADCP) measurements of turbidity currents were collected just 6 km offshore from the river mouth. This ADCP mooring deployment is closer to the river mouth than used by Khripounoff et al. (2009; 2012), and allows us to monitor the proximal velocity structure of the Var Canyon turbidity currents in unprecedented detail. We use these measurements to test the link between river floods and velocity structure of the turbidity currents. More specifically, we test whether the previously proposed criteria indeed distinguish flood-triggered turbidity currents from other triggers, at locations close to the river mouth. We then use a second mooring farther offshore (16 km) to test whether such proximal velocity structure is preserved down-canyon. Finally, we discuss the implications of these findings for reconstructing paleo-flood records from turbidity-current deposits.

TERMINOLOGY

Confusion can occur if terms are not clearly defined, and terms such as “hyperpycnal” have been used by different authors in somewhat different ways (Shanmugam, 2018; Feng, 2019; Zavala, 2019). We therefore specify the terminology used throughout this paper. We define a *turbidity current* as a gravity-driven subaqueous sediment density flow, where the dominant particle support is fluid turbulence (Mulder and Alexander, 2001), although turbulence may be damped in near-bed layers that characterize high-density turbidity currents (Lowe, 1982; Kneller and Branney, 1995; Cantero et al.,

2012; Eggenhuisen et al., 2017). We call a turbidity current "*flood-triggered*" if sediment suspended during a river flood (a distinct, sharp peak in river discharge) directly transfers into the turbidity current. Such direct transfer of flood-derived sediment could occur via two of the earlier-mentioned mechanisms; instantaneously via plunging (Mulder et al., 2003) or via concentrated pockets of sediment in convective fingers (Parsons et al., 2001). We reserve the term "*hyperpycnal turbidity currents*" for turbidity currents that are direct continuations of plunging rivers (Talling, 2014). All non-flood-triggered turbidity currents occurring in a river-fed submarine channel are here labelled as *"river-associated*" turbidity currents and include flows triggered by tides (Hage et al., 2019) and submarine landslides (Hughes Clarke et al., 2014). More specifically, we use the term "*landslide-triggered*" for surge-like turbidity currents, commonly assumed to be of short duration due to non-permanent sediment supply (Mulder and Alexander, 2001), and consisting of a sudden onset with high-velocity front and a subsequent waning flow (Kneller and Buckee, 2000). The term "*velocity structure"* is used for a time series of velocity measured at a single spatial point (e.g., mooring). Merging of pulses (distinct velocity peaks) in the velocity time series is referred to as "*amalgamation"*.

STUDY AREA

The Var Canyon is located offshore Nice in the Mediterranean Sea, and extends for approximately 20 km before joining with the Paillon Canyon at 1850 m water depth (Fig. 1A; Piper and Savoye, 1993). The Var Canyon begins directly at the Var River mouth. The Var River discharge has a yearly cyclicity of enhanced discharge in the spring and summer due to snow melt, followed by high-intensity rainfall floods separated by low river discharges during the winter (Mulder et al., 1998). The average annual discharge is 50 $m^3 s^{-1}$, with the biannual flood recurrence at 810 $m^3 s^{-1}$ (http://www.hydro.eaufrance.fr).

The Var Canyon turbidity-current activity is well known from the large landslide-triggered turbidity current that occurred during the construction of Nice Airport in 1979 (Mulder et al., 1997).

159 Khripounoff et al. (2009, 2012) published the only studies in the Var Canyon that used direct velocity
160 measurements of turbidity currents in this system. They found that in the canyon several turbidity
161 currents are initiated each year either by river floods or submarine landslides (Khripounoff et al.,
162 2012). Typical turbidity current velocities are from 20 to 90 cm s^{-1}, with a duration between 4 and 24
163 hours, and a flow thickness between 50 and 130 m (Khripounoff et al., 2009, 2012). In the Var
164 Canyon, flood-triggered turbidity currents are found to have the lowest velocities, shortest duration,
165 and highest vertical extent (Table 1 in Khripounoff et al., 2012).

166 ## METHODS

167 Here we analyze a new dataset from the Var River-Canyon system that was collected during the
168 Solveig III research cruise, acquired over a period of seven months, from late June 2009 to early
169 February 2010 (Fig. 2; Blandin, 2010). We first compare velocity data from a proximal canyon
170 mooring to river discharge measurements, to analyze the relationship between the velocity structure of
171 turbidity currents and associated river discharge. We then use a second mooring to trace the changes
172 in the velocity structure of the turbidity currents down the canyon. Another, third mooring was located
173 directly offshore the river mouth (2.8 km), but it unfortunately was located just outside the deepest
174 part of the canyon floor (thalweg) and consequently did not record any turbidity currents.

175 ### *Land Stations*

176 Var River discharges were recorded at the NapoleonIII site (Nice, France; Fig. 1A) every 15 minutes
177 (HYDRO http://www.hydro.eaufrance.fr). Near Nice Airport, a MeteoFrance weather station recorded
178 hourly maximum wind speeds based on 10-minute average values, as well as precipitation on an
179 hourly basis (Fig. 2A).

180 ### *Var Canyon Mooring Configuration*

181 Initially three moorings (VH, VV, VE) were deployed in the Var Canyon (Fig. 1A, B). The shallowest
182 mooring (VH) was potentially located outside the deepest part of the canyon thalweg (Fig. 1B). It is
183 especially challenging to deploy moorings precisely in the thalweg center in this narrow proximal part
184 of the canyon. Consequently, the exact seabed location of mooring VH in relation to the channel

thalweg remains uncertain, due to the potential offset between the release location of the mooring and its final landing location. This mooring did not measure any turbidity currents, but the mooring set-up and the resulting data are still presented briefly here to provide a complete overview of the observations. However, these observations are not analyzed in as much detail as those from the other moorings, which were located in the thalweg. Most instruments on the moorings recorded at a 20-minute interval, unless stated otherwise.

Station VH was located on the side wall of the submarine canyon at 121 meters water depth (mwd), and 2.8 km from NapoleonIII measurement station at the river mouth (Fig. 1A, B). On this mooring, there was a Seaguard Recording Current Meter (RCM) at 15 meters above the seafloor (masf), an RCM 11 at 25 masf that recorded every 5 minutes, and an Aquadopp RCM at 35 masf recording at 30 min intervals (Fig. 1C).

Station VE was deployed at 518 mwd, at a location 5.7 km from NapoleonIII (Fig. 1A, B). Mooring VE had a turbidity sensor mounted at 15 masf (Fig. 1C). A 300 kHz acoustic Doppler current profiler (ADCP) was mounted at 30 masf, which recorded over a series of 2-m-high bins. Besides the maximum velocity, the velocity at 25 masf is also extracted from the ADCP data to enable a direct comparison between the depth-resolved ADCP data and the single depth point RCM measurements on the other moorings. A sediment trap (PPS 4/3-Technicap) was mounted at 40 masf. Settling particles were collected over a 9-day window using cylindrical sediment traps with a sampling aperture of 0.05 m^2. These traps were covered with a honeycomb baffle with 10-cm-deep cells, which were 1 cm in diameter, and were equipped with 24 sampling bottles.

Station VV was located at 1280 mwd, 15.7 km away from the river mouth (Fig. 1A, B). Here, the sediment trap was located at 15 masf (Fig. 1C), with the same specifications and set-up as at station VE. A RCM 11 was installed at 25 masf. An additional mooring with a 75 kHz ADCP, at 220 masf, was deployed at the same location. The height of this mooring allows the calculation of flow thickness, using calculations of depth-averaged height following the integral definition of Stacey and Bowen (1988). This ADCP recorded every 5 minutes, and had a 6 m vertical bin size.

211 Sediment concentrations in the flows were also estimated using backscatter data of the 300 kHz
212 ADCP at station VE. This provides further information on first-order flow character, but involves a
213 significant assumption that grain size does not vary with height above the bed (see Simmons et al.
214 (2020) for a detailed description of likely errors associated with this assumption). However, it is
215 established that grain size will increase towards the bed, with grain-size stratification depending on
216 the Rouse number and other factors (e.g., Kneller and Buckee, 2000; Eggenhuisen et al., 2020). Due
217 to this simplification, the primary conclusions from this contribution are thus based only on ADCP
218 velocity measurements, with the sediment concentrations contributing further information on flow
219 properties. Briefly, the backscatter data were converted to sediment concentration using an implicit
220 inversion method, with an iterative method of accounting for sediment attenuation (see Thorne and
221 Hanes (2002) for a detailed description of the method). The intensity of the acoustic backscatter
222 depends on both grain size of the suspended particles, as well as sediment concentration. When using
223 a single-frequency ADCP, a vertical grain-size profile needs to be assumed for each measurement in
224 the flow (Simmons et al., 2020). This grain size can be derived from sediment cores or traps (cf.
225 Azpiroz-Zabala et al., 2017). Here, we assume a single grain-size value for all vertical profiles, as
226 vertical grain-size stratification in the flow cannot be quantified on the basis of sediment-trap samples
227 available here. The sediment-trap samples used for grain-size estimates came from the Solveig I
228 cruise (Silva Jacinto, 2008) between late November 2008 and early December 2008. The Solveig III
229 sediment trap samples were used for destructive sampling of carbon, so they were unavailable for
230 grain-size measurements. During the Solveig I cruise, a sediment trap was located near the river
231 mouth, at 500 mwd, and it returned a mean grain size of 40 μm. Furthermore, estimates of sediment
232 concentration presented here assume that the ADCP constant (K_t) is 2.31 x 10^7 (Simmons et al.,
233 2020). The 75 kHz ADCP data, near station VV, is not used for conversion of acoustic backscatter to
234 sediment concentrations, as there was no (K_t) calibration value available for an instrument with
235 similar frequency.

236

RESULTS

Var River Observations

The river discharge followed its standard yearly cycle comprising a long-duration snowmelt peak over the spring and summer, and high-intensity rainfall floods during winter (Fig. 2A). During the initial four months from July to September 2009, the river discharge gradually declined from 200 $m^3 s^{-1}$ to 80 $m^3 s^{-1}$. Four winter floods occurred during the deployment (Fig. 2A). Two of these river-mouth floods exceeded 200 $m^3 s^{-1}$, with a peak discharge of 250 $m^3 s^{-1}$ in October 2009, and a maximum peak discharge of 765 $m^3 s^{-1}$ that occurred on December 2009. These two floods also correspond to increases in offshore flow velocities in the Var Canyon, indicating that turbidity currents were initiated in the Canyon (Fig. 2; events no. 4 and 5). The other two peaks in river discharge occurred in September and November 2009, with significantly lower discharges (86 and 105 $m^3 s^{-1}$), and did not produce turbidity currents at the seafloor moorings. Analysis of the local wind speed did not yield any correlation between the occurrence of turbidity currents and high wind speeds, although the October 2009 event was preceded by a storm day (Fig. 2A, blue line).

Var Canyon Observations

At the most proximal station VH, there was a notable lack of observable turbidity-current activity, with velocities limited to 20 cm s^{-1} (Fig. 2B). It is most likely that the flows were not recorded at station VH because of its misplacement (Fig. 1B). Alternatively, either the proximal turbidity currents were not thick enough to reach the current meters placed at 15 masf, or the sediment plume from the river bypassed this VH mooring and flows started farther down-canyon. Given the off-center release location, the narrow V-shaped canyon shape, and the total lack of velocity, temperature, and turbidity signals, it is most likely that the mooring was misplaced.

Station VE (ADCP data) and VV (RCM current meter data) recorded five separate turbidity currents, which are termed flows 1, 2, 3, 4, and 5 (Fig. 2). Flows 2 and 3 were recorded only at a single mooring, and are considered to be minor local events, as neither flow led to increased sediment flux in traps (Fig. 2C, D). The three remaining events (flows 1, 4, and 5) did lead to an increased sediment

263 flux, and were recorded by both mooring station VE and VV (Fig. 2; Table 1). These three flows are
264 now discussed in more detail (Figs. 3, 4).

265 **July 2009 Event (Event 1).---**

266 This turbidity current lasted from 30 June to 5 July 2009. During this period, the Var River lacked a
267 distinct flood peak (Fig. 3A). Instead, the river's discharge (~ 80 m^3 s^{-1}) continued a gradual decline
268 following the peak snow melt in early spring (Fig. 2). Previous measurements have shown that
269 comparable discharge levels in the Var River correspond to suspended-sediment concentration of up
270 to 3 kg m^{-3} based on previous direct river measurements (Mulder et al. 1998).

271 At station VE, the July turbidity current lasted for nearly 3.5 days (Table 1). The velocity signal, as
272 well as the sediment concentration, were characterized by a gradual onset followed by a long
273 continuous series of pulses (Figs. 3, 4). Velocities and sediment concentrations gradually rose until a
274 peak velocity of 35 cm s^{-1} occurred after roughly 1.3 days. Event 1 was not associated with an
275 increase in temperature at station VE (Fig. 3B).

276 Ten kilometers farther down canyon, at station VV, the July event reorganized in three distinct pulses,
277 each lasting for ~ 5-10 hrs. All these pulses show a sharp increase in velocity and temperature at the
278 start of the flow followed by a gradual decline (Fig. 3C). The peak velocities are similar to those
279 measured in the proximal station (Table 1, Fig. 3). The transit velocity between station VE and VV is
280 particularly slow at ~ 7 cm s^{-1}, suggesting that the first velocity peaks observed in VE dissipated
281 before reaching station VV. The transit velocity would be more in agreement with the direct velocity
282 measurements if a later velocity peak from station VE is considered to arrive first at station VV, and
283 earlier peaks dissipated between VE and VV.

284 **October 2009 Event (Event 4).---**

285 Flow 4 in October 2009 coincided with a Var River flood with a discharge peak of 250 m^3 s^{-1} (Fig.
286 3A), equating to a suspended sediment concentration in the river of ~ 8 kg m^{-3} based on the Var River
287 rating coefficient (Mulder et al., 1998). At station VE, the duration of the event was between 20 and
288 24 hours (Table 1). The velocity structure and sediment concentration consist of a sudden onset

289 followed by a complex series of higher and lower pulses (Figs. 3B, 4B). A peak velocity of 62 cm s^{-1}
290 occurs at the front of the turbidity current.

291 At station VV, the flow duration was reduced by 50% to 10-13 hours (Figs. 3C, 4C, Table 1). The
292 turbidity current is characterized by a single pulse with an abrupt onset. The velocity peaks at 30 cm s^{-1}
293 at the start of the event, followed by a steady decline in velocity. Again, the increase in velocity at
294 station VV is paired with an increase in temperature (Table 1, Fig. 3). The transit velocity between
295 these two moorings, at 76 cm s^{-1}, indicates an acceleration of the turbidity current before its arrival at
296 station VV.

297 **December 2009 Event (Event 5).---**

298 Event 5 is associated with the largest flood observed during this seven-month deployment (Fig. 2).
299 This flood consisted of two stages, and occurred between 23 and 26 December. In the first stage (23rd
300 December), the river discharge increases over an ~ seven-hour window up to a peak discharge of ~
301 240 m^3 s^{-1} (Fig. 3A). This first peak is followed by a 28-hour period in which an elevated river
302 discharge of ~ 120 m^3 s^{-1} was maintained. In the second stage (25th December), the flood reached its
303 maximum discharge of ~ 765 m^3 s^{-1} in 10 hours (Fig. 3A). Overall the second-stage flood lasted for
304 about 39 hours, and the entire duration of elevated discharge during the December event was ~ 3.5
305 days. Estimation of the suspended-sediment concentration by extrapolating the rating curve of the
306 river indicate that sediment concentrations of 20-50 kg m^{-3} are likely to have occurred during the
307 second stage of the flood. Such levels of suspended sediment could be sufficient for the formation of a
308 hyperpycnal turbidity current (Mulder et al., 1998).

309 At station VE, the measured velocities of the December event mirror the two-stage river discharge
310 curve. On the 23rd of December, following the first stage of the river flood, a sharp increase in the
311 velocity and sediment concentration is observed at VE (Figs. 3B and 4B). The sharp increase is
312 followed by several lower velocity peaks until the second stage. As the river reaches its maximum
313 discharge on the 25th of December, a series of new and higher velocity peaks are recorded at station
314 VE. This second stage lasts for about 42 hours, has a sharp onset, with a further increase in sediment
315 concentration, and reaches its peak velocity (102 cm s^{-1}) about 7 hours after the start of this second

316 stage (Figs. 3B, 4B; Table 1). Interestingly, the second stage of the December event is the only event
317 that is significantly warmer than the ambient water at station VE.

318 The velocity peaks of the first stage of the December event are not observed at station VV. The arrival
319 of the second stage is marked by a sharp increase in the velocity to its peak value of 85 cm s^{-1}, which
320 is followed by a continuous decrease lasting about 13 hours. In the following 3-4 days, multiple re-
321 surging phases occur (Figs. 3C, 4C).

322 The transit velocity between station VE and VV, based on the first arrival time at either station, is 65
323 cm s^{-1}. The observed maximum velocity peak at station VE (102 cm s^{-1}) occurs after the arrival of the
324 front peak at the more distal station VV, and hence this proximal maximum velocity peak cannot be
325 the distal maximal velocity peak. This observation implies that the maximum velocity peak at VE is
326 not maintained down-canyon, but instead this proximal maximum velocity peak dissipates and
327 becomes just a minor velocity peak at station VV.

328

329 **DISCUSSION**

330 *Is There a Unique Proximal Structure of Flood-Triggered Turbidity Currents?*

331 Four criteria have been proposed as diagnostic features of flood-triggered turbidity currents. These
332 include a long duration, gradual onset, possible multiple cycles, and relatively low velocities
333 (Khripounoff et al., 2012; Zavala and Pan, 2018, Mulder et al., 2003). All turbidity currents observed
334 in the proximal station in the Var Canyon display at least two of these characteristics, as all events (1,
335 4, 5) consist of multiple cycles and have a long duration in comparison to previous measurements in
336 the Var Canyon (Khripounoff et al., 2012). The July event (event 1) was the only turbidity current
337 with a gradual onset, and had low velocities in comparison to both the October and December events
338 (events 4 and 5) as well as compared to events reported by Khripounoff et al. (2012). Thus, all three
339 measured events at the proximal mooring show reasonable agreement with the four criteria set out for
340 flood-triggered turbidity currents. Importantly, the July event does not coincide with a river flood,
341 although the other two events are linked to floods (Fig. 3).

342 Although the July event (event 1) fits the flood-triggered criteria best, it lacks any association with a
343 flood (Fig. 3A). However, during the October and December events the river floods produced
344 sufficiently high suspended-sediment concentrations (4-8 kg m^{-3} for October and 20-50 kg m^{-3} for
345 December; Table 1) to enable direct transfer of suspended sediment from the river to the turbidity
346 current. For both October and December events, the sediment transfer could have occurred through
347 convective fingering (Parsons et al., 2001). Additionally, the second stage of the December event
348 (event 5) could be a hyperpycnal turbidity current, as the sediment concentration is sufficient for the
349 river discharge to plunge and move along the seabed. Such a hyperpycnal trigger would be consistent
350 with the unique increase in temperature observed at VE during this second stage.

351 The July event lacks a clear river flood (event 1, Figs. 2 and 3). Yet, during the July event the
352 suspended-sediment levels in the river discharge are estimated to be up to 3 kg m^{-3} (Table 1), which is
353 still sufficient to form convective fingers (Mulder et al., 1998; Parsons et al., 2001). However, the
354 river discharge measurements indicate that similar or higher levels of sediment concentration are
355 expected continuously in the weeks leading up to the July event (Fig. 3A). Thus, if convective fingers
356 were responsible for the transfer of sediment from the river to the submarine canyon, this should have
357 resulted in continuous turbidity-current activity over the weeks leading up to the event. Such
358 continuous turbidity-current activity was observed neither in the weeks leading up to the July event,
359 nor in earlier measurements of Khripounoff et al. (2009) during similar conditions in the years 2006
360 and 2007. It is more likely that the July event was initiated by some form of landslide, which
361 generated a relatively sustained flow at the proximal VE station (Fig. 3B). One possible hypothesis is
362 that this turbidity current was triggered by retrogressive breaching failure, which can lead to
363 continuous sediment supply and thus prolonged flow (Mastbergen and Van Den Berg, 2003). The July
364 event fits the flood-triggered criteria best (gradual onset, multiple cycles, low velocity, and long
365 duration). Thus, it is important that this July event was most likely triggered by a landslide. Although
366 the flood-triggered criteria are present in the Var Canyon observations, these criteria might not be
367 unique to flood triggers.

How Does the Proximal Velocity Structure Evolve Down-Canyon?

We now discuss how the proximal velocity structure of the flows evolved and changed with distance, what controls the evolution of this velocity structure, and its implications for inferring triggers from grain-size patterns in deposits.

The typical proximal velocity structure observed in station VE is different from the typical velocity structure seen 10 km farther down canyon. At the proximal VE station, the three main events (1, 4, 5) all show multiple cycles of acceleration and deceleration (pulses). However, at the 10 km more distal VV station, these multi-pulsed turbidity currents have self-organized to distinct single velocity peaks. For the October and December events, the flow reorganized to one distinct pulse, whilst the July event shows three distinct velocity peaks. These reorganized flow structures at the most distal VV station all show a dominant velocity peak at the front of the flow, followed by a steady decline; as typically expected for landslide-triggered turbidity currents (Kirwan et al., 1986; Normark and Piper, 1991; Kneller and Buckee, 2000; Mulder et al., 2003). This down-canyon transformation, from multi-pulsed to single-pulsed turbidity current, is consistent with field observations of Kneller and McCaffrey (2003) and laboratory experiments of Ho et al. (2018). Kneller and McCaffrey (2003) suggest that merging of velocity pulses can lead to simplified normally graded deposits towards the end of a canyon or channel system. Ho et al. (2018) also found that amalgamation of multi-pulsed flows is likely, as faster pulses within the flow experience a reduction in drag and consequently experience a forward advection to the flow front. The reduced drag is caused by the stratified water column that remained after the passage of the first pulse (Ho et al., 2018). The results shown here suggest that this amalgamation of pulses in the Var Canyon system is extremely efficient, leading to flooding signals effectively shredded within the first 16 km of the submarine canyon system.

However, the field observations also show that amalgamation of pulses is not as straightforward as seen in laboratory experiments. For example, during the second stage of the December event (25th of December onwards), the fastest peak is unable to catch up with the slower leading peak. Although this originally higher-velocity peak from station VE is discernible 10 km downstream, it is now slower than the frontal peak. This suggests that amalgamation of individual flow pulses also depends on other

factors besides reduced drag. We propose that the pulse propagation also depends on availability of easily erodible substrate on the seafloor. For the second stage of the December event, the frontal pulse might have eroded the sediment freshly deposited by the first stage, causing the observed self-acceleration. Subsequently, the depleted seafloor could not fuel the following higher velocity peaks, resulting in deceleration of those initially higher velocity peaks. The importance of erosion and the state of the seafloor is consistent with previous observations. For example, Liu et al. (2012) documented that the first typhoon of the season produces the strongest turbidity current, Hage et al. (2019) showed that the first low tide of the spring cycle produces a fast and erosive turbidity current, and Heerema et al. (2020) showed that the first event after a prolonged quiescent period triggers the most ignitive flow. Overall, here in the Var Canyon the combined effect of erosion and amalgamation results in shredding of the flood signal within 16 km of the river mouth.

Further Implications for Identifying Turbidity Currents Triggered by River Floods

The Applicability of Depositional Models.---

We now use our direct measurements to assess existing depositional models for flood-triggered events. The processes underpinning these models have been heavily debated (e.g., Shanmugam, 2018; van Loon et al., 2019; Zavala, 2019), and have led to three competing depositional models (Mulder et al., 2003; Plink-Björklund and Steel, 2004; Nakajima, 2006; Talling, 2014). Central to the initial model from Mulder et al. (2003) is that waxing and waning of the river flood causes a waxing and waning turbidity-current velocity structure, and this is subsequently recorded in deposits via inverse-to-normal grading. This model suggests that the gradual rising limb of the river leads to a gradual increase in the velocity of the turbidity current, which in turn is recorded as a coarsening-upward (inversely graded) sequence in the deposits. Next, the falling limb of the flood produces a gradual decrease of the turbidity-current velocity that produces an upward-fining (normally graded) deposit. Later models of Plink-Björklund and Steel (2004) and Zavala et al. (2006) include incremental deposition of thick sandy deposits due to prolonged duration of hyperpycnal events. This in contrast to a third model that suggests that flood-triggered turbidity currents form thin, fine-grained deposits,

422 due to the slow and dilute nature of flood-triggered turbidity currents (Nakajima, 2006; Talling,
423 2014).

424 In our direct measurements, we do indeed find prolonged durations of flood-triggered events 4 and 5.
425 These events last up to four days, and could lead to thick deposits as suggested by Plink-Björklund
426 and Steel (2004) and Zavala et al. (2006). The variable peak velocities (26 - 102 cm s^{-1}) between the
427 measured events could be consistent with both the proposed sandy beds (Plink-Björklund and Steel,
428 2004; Zavala et al., 2006), as well as finer silt beds (Nakajima, 2006; Talling, 2014). However, the
429 velocity onset of the events tends to be abrupt, especially at the distal station, suggesting that the
430 inverse grading proposed by Mulder et al. (2003) becomes less likely with distance from the river
431 mouth.

432 Notably, multiple inversely graded deposits are found on a terrace in the Var Canyon at ~ 30 km from
433 the Var River mouth, and are interpreted to reflect river-triggered turbidity currents (Mulder et al.,
434 2001). These findings conflict with our measurements that demonstrate efficient self-organization of
435 turbidity currents within 16 km from the Var River mouth. The existence of these inversely graded
436 deposits of Mulder et al. (2001) suggest that some events retain their gradual velocity onset farther
437 down-canyon, leading to these distal inversely graded deposits. Such flows are assumed to have lasted
438 longer, reaching their peak velocity later, and hence would have required more time to self-organize;
439 they may represent larger floods that are more prolonged. Therefore, these events would carry the
440 waxing signal over greater distances, to form distal inversely graded deposits. Such events may be
441 relatively infrequent, at least compared to the flow types measured in this study. The persistence of
442 these inversely graded deposits farther offshore suggests that the recent direct monitoring
443 observations do not yet include lower-frequency turbidity currents (Mas et al., 2010).

444 Some insights into the dynamics of such possible high-magnitude flows might be gained from the
445 large hyperpycnal turbidity current in December. Proximally, this event does indeed have a gradual
446 onset, as peak velocity occurs ~ 7 hours after the start of the event. However, amalgamation prevents
447 the preservation of this gradual onset farther downstream. Interestingly, the large hyperpycnal event
448 (maximum river discharge 610 m^3 s^{-1}) measured by Khripounoff et al. (2012) on December 15, 2008,

449 shows that amalgamation is not always able to completely reorganize turbidity currents within the
450 first 16 km. The December 2008 event of Khripounoff et al. (2012) shows how a large flood-triggered
451 flow generally resembles a landslide-triggered flow in terms of its velocity structure at location VV,
452 just like the events presented here. However, this December 2008 event still consists of two distinct
453 peaks at station VV (Khripounoff et al., 2012). The second, faster, peak is projected to catch up within
454 5-10 km to finalize self-organization into a single-peak, surge-type flow, based on their peak velocity
455 and arrival times. Potentially, the incomplete amalgamation observed by Khripounoff et al. (2012)
456 could be due to the fact that the rising limb of that December 2008 event lasted twice as long as the
457 December 2009 flood presented here. It may thus be possible that during even longer river floods, the
458 flood-triggered velocity structure is preserved farther offshore, thereby explaining the inversely
459 graded deposits observed by Mulder et al. (2001).

460 In summary, all three depositional models are to some extent consistent with our direct measurement
461 observations of flood-triggered events. Flood-triggered events could indeed result in sustained flows,
462 indicated by traction structures, such as climbing ripples or plane-parallel lamination (Plink-Björklund
463 and Steel, 2004; Zavala et al., 2006). Especially proximally, large flood-triggered events could also
464 result in inversely-to-normally graded sequences (Mulder et al., 2003), and vertical alternation of
465 traction structures reflecting cyclicity in the flow (Nakajima, 2006; Zavala et al., 2006). Although all
466 proposed models work for some flows, it should be kept in mind that none of these depositional
467 models apply exclusively to all flood-triggered flows. Furthermore, events without a flood trigger can
468 also (partially) fulfill the proposed criteria for flood-triggered events. Finally, as previously suggested
469 by Kneller and McCaffrey (2003), vertical-grading patterns in deposits are expected to simplify with
470 distance from source, due to amalgamation of the velocity pulses over distance. This merging of
471 velocity pulses leads to a simplified normal grading in distal positions. In this study, we show that this
472 simplification can occur rapidly, within 16 km from the river mouth.

473

How Reliable Is the Depositional Record for Reconstructing Paleo-Floods?.---

Turbidite records of paleo-floods have been used to reconstruct recurrence levels of river flooding (Mulder et al., 2001; Nakajima, 2006), and to understand the effects of sea-level change on river floods (Plink-Björklund and Steel, 2004). However, this study has shown that although the velocity structure of flood-triggered turbidity currents is consistent with the proposed criteria, this structure is not unique to flood-triggered events (Fig. 5). For instance, initially multi-pulsed and prolonged velocity structures have been observed without a flood, as in the landslide-triggered July event (event 1). Moreover, similar river discharge levels have not consistently led to turbidity currents in the canyon. For example, Khripounoff et al. (2012) observed a 640 $m^3 s^{-1}$ river flood that did not immediately lead to a turbidity current, whilst a 610 $m^3 s^{-1}$ river flood did directly produce a turbidity current. Additionally, three similar river floods of ~ 250 $m^3 s^{-1}$ led to substantially different turbidity current activity. A first flood (230 $m^3 s^{-1}$) described in Khripounoff et al. (2012) did not lead to any activity. A second flood (240 $m^3 s^{-1}$) during the first phase of the December event (described here) led to activity only at the first mooring. Lastly, the October flood (250 $m^3 s^{-1}$, described here) triggered an event that was observed at all mooring stations. Thus, recognition of paleo-floods based only on velocity structure and subsequent grain size trends might be problematic. Additional indicators, such as substantial organic-matter content with high carbon-nitrogen ratio, could be needed to confidently infer flood triggers. However, this may also be problematic, as seabed failures on the delta may also remobilize recently deposited sediment with similarly high organic-carbon contents or carbon-nitrogen rations.

Finally, it has been suggested that peaks in earthquake shaking patterns (seismograms) can also produce multi-pulsed turbidity currents (Howarth et al., 2021), and that turbidites with multiple pulses may be diagnostic of earthquake triggering (Goldfinger et al., 2003). This study emphasizes that river floods can also produce multi-pulsed turbidity currents, and presumably multi-pulsed turbidites, and that amalgamation of initial pulses can occur over distances of < 16 km. Both of these points may complicate the discrimination of earthquake and flood-triggered turbidity currents (Talling, 2021).

CONCLUSIONS

Turbidity currents without a flood trigger can resemble flood-triggered turbidity currents (Fig. 5), potentially due to a seafloor failure followed by sustained breaching. In addition, flood-triggered turbidity currents can look like landslide-triggered turbidity currents, as erosion and amalgamation in turbidity currents lead to self-organization of the flow within tens of kilometers. Lastly, similar river flood discharges do not consistently lead to similar turbidity currents. Thus, reconstructing paleo-floods on the basis of the rock record might prove substantially more complicated than previously assumed.

ACKNOWLEDGMENTS

We thank the crew members of the Solveig III cruise, as well as all technicians and the scientific team involved in the efforts. CJH is funded by the European Union's Horizon 2020 research and innovation program under the Marie Skłodowska-Curie grant agreement No 721403 - ITN SLATE. MJBC was supported by a Royal Society Research Fellowship (DHF/R1/180166).

References

Azpiroz-Zabala, M., Cartigny, M.J.B., Talling, P.J., Parsons, D.R., Sumner, E.J., Clare, M.A., Simmons, S.M., Cooper, C., and Pope, E.L., 2017, Newly recognized turbidity current structure can explain prolonged flushing of submarine canyons: Science Advances, v. 3, no. e1700200.

Bailey, L.P., Clare, M.A., Rosenberger, K.J., Cartigny, M.J., Talling, P.J., Paull, C.K., Gwiazda, R., Parsons, D.R., Simmons, S.M., Xu, J., Haigh, I.D., Maier, K.L., McGann, M., Lundsten, E., and Monterey CCE Team, 2021, Preconditioning by sediment accumulation can produce powerful turbidity currents without major external triggers: Earth and Planetary Science Letters, v. 562, no.116845.

Blandin, J., 2010, SOLVEIG III cruise, L'Europe R/V.

Cantero, M.I., Cantelli, A., Pirmez, C., Balachandar, S., Mohrig, D., Hickson, T.A., Yeh, T., Naruse, H., and Parker, G., 2012, Emplacement of massive turbidites linked to extinction of turbulence in turbidity currents: Nature Geoscience, v. 5, p. 42–45.

Eggenhuisen, J.T., Cartigny, M.J.B., and de Leeuw, J., 2017, Physical theory for near-bed turbulent particle suspension capacity: Earth Surface Dynamics, v. 5, p. 269–281.

Eggenhuisen, J.T., Tilston, M.C., Leeuw, J., Pohl, F., and Cartigny, M.J.B., 2020, Turbulent diffusion modelling of sediment in turbidity currents: An experimental validation of the Rouse approach: The Depositional Record, v. 6, p. 203–216.

Feng, Z.-Z., 2019, Words of the Editor-in-Chief —— some ideas about the comments and discussions of hyperpycnal flows and hyperpycnites: Journal of Palaeogeography, v. 8, p. 25.

Galy, V., France-Lanord, C., Beyssac, O., Faure, P., Kudrass, H., and Palhol, F., 2007, Efficient organic carbon burial in the Bengal fan sustained by the Himalayan erosional system: Nature, v. 450, p. 407–410.

539 Gavey, R., Carter, L., Liu, J.T., Talling, P.J., Hsu, R., Pope, E., and Evans, G., 2017, Frequent
540 sediment density flows during 2006 to 2015, triggered by competing seismic and weather events:
541 Observations from subsea cable breaks off southern Taiwan: Marine Geology, v. 384, p. 147–158.

542 Goldfinger, C., Nelson, C.H., Johnson, J.E., and Shipboard Scientific Party, 2003, Holocene
543 earthquake records from the Cascadia subduction zone and northern San Andreas fault based on
544 precise dating of offshore turbidites: Annual Review of Earth and Planetary Sciences, v. 31, p.
545 555-577.

546 Hage, S., Cartigny, M.J.B., Sumner, E.J., Clare, M.A., Hughes Clarke, J.E., Talling, P.J., Lintern,
547 D.G., Simmons, S.M., Silva Jacinto, R., Vellinga, A.J., Allin, J.R., Azpiroz-Zabala, M., Gales,
548 J.A., Hizzett, J.L., Hunt, J.E., Mozzato, A., Parsons, D.R., Pope, E.L., Stacey, C.D., Symons,
549 W.O., Vardy, M.E., and Watts, C., 2019, Direct Monitoring Reveals Initiation of Turbidity
550 Currents From Extremely Dilute River Plumes: Geophysical Research Letters, v. 46, p. 11.310–
551 11.320.

552 Heerema, C.J., Talling, P.J., Cartigny, M.J., Paull, C.K., Bailey, L., Simmons, S.M., Parsons,
553 D.R., Clare, M.A., Gwiazda, R., Lundsten, E., Anderson, K., Maier, K.L., Xu, J.P., Sumner, E.J.,
554 Rosenberger, K., Gales, J., McGann, M., Carter, L., and Pope, E., 2020, What determines the
555 downstream evolution of turbidity currents? Earth and Planetary Science Letters, v. 532, no.
556 116023.

557 Ho, V.L., Dorrell, R.M., Keevil, G.M., Burns, A.D., and McCaffrey, W.D., 2018, Pulse
558 propagation in turbidity currents (J. Baas, Ed.): Sedimentology, v. 65, p. 620–637.

559 Howarth, J.D., Orpin, A.R., Kaneko, Y., Strachan, L.J., Nodder, S.D., Mountjoy, J.J., Barnes,
560 P.M., Bostock, H.C., Holden, C., Jones, K. and Cağatay, M.N., 2021, Calibrating the marine
561 turbidite palaeoseismometer using the 2016 Kaikōura earthquake: Nature Geoscience, v. 14, p.
562 161–167.

563 Hughes Clarke, J.E., 2016, First wide-angle view of channelized turbidity currents links migrating
564 cyclic steps to flow characteristics: Nature Communications, v. 7, p. 11896.

565 Hughes Clarke, J.E.H., Marques, C.R.V., and Pratomo, D., 2014, Imaging Active Mass-Wasting
566 and Sediment Flows on a Fjord Delta, Squamish, British Columbia, *in* Krastel, S., Behrmann, J.-
567 H., Völker, D., Stipp, M., Berndt, C., Urgeles, R., Chaytor, J., Huhn, K., Strasser, M., and
568 Harbitz, C.B. eds., Submarine Mass Movements and Their Consequences: Cham, Springer
569 International Publishing, Advances in Natural and Technological Hazards Research, v. 37, p.
570 249–260.

571 Khripounoff, A., Vangriesheim, A., Crassous, P., and Etoubleau, J., 2009, High frequency of
572 sediment gravity flow events in the Var submarine canyon (Mediterranean Sea): Marine Geology,
573 v. 263, p. 1–6.

574 Khripounoff, A., Crassous, P., Lo Bue, N., Dennielou, B., and Silva Jacinto, R., 2012, Different
575 types of sediment gravity flows detected in the Var submarine canyon (northwestern
576 Mediterranean Sea): Progress in Oceanography, v. 106, p. 138–153.

577 Kirwan A.D., Jr., Doyle, L.J., Bowles, W.D., and Brooks, G.R., 1986, Time-Dependent
578 Hydrodynamic Models of Turbidity Currents Analyzed with Data from the Grand Banks and
579 Orleansville Events: Journal of Sedimentary Petrology, v. 56, p. 379-386.

580 Kneller, B.C., and Branney, M.J., 1995, Sustained high-density turbidity currents and the
581 deposition of thick massive sands: Sedimentology, v. 42, pp.607-616.

582 Kneller, B.C., and Buckee, C., 2000, The structure and fluid mechanics of turbidity currents: a
583 review of some recent studies and their geological implications: Structure of turbidity currents:
584 Sedimentology, v. 47, p. 62–94.

585 Kneller, B.C., and McCaffrey, W.D., 2003, The Interpretation of Vertical Sequences in Turbidite
586 Beds: The Influence of Longitudinal Flow Structure: Journal of Sedimentary Research, v. 73, p.
587 706–713.

588 Lintern, D.G., Hill, P.R., and Stacey, C., 2016, Powerful unconfined turbidity current captured by
589 cabled observatory on the Fraser River delta slope, British Columbia, Canada (P. Talling, Ed.):
590 Sedimentology, v. 63, p. 1041–1064.

591 Liu, J.T., Wang, Y.-H., Yang, R.J., Hsu, R.T., Kao, S.-J., Lin, H.-L., and Kuo, F.H., 2012,
592 Cyclone-induced hyperpycnal turbidity currents in a submarine canyon: Journal of Geophysical
593 Research: Oceans, v. 117, no. C04033.

594 Lowe, D.R., 1982, Sediment Gravity Flows: II Depositional Models with Special Reference to the
595 Deposits of High-Density Turbidity Currents: Journal of Sedimentary Petrology, v. 52.

596 Mas, V., Mulder, T., Dennielou, B., Schmidt, S., Khripounoff, A., and Savoye, B., 2010,
597 Multiscale spatio-temporal variability of sedimentary deposits in the Var turbidite system (North-
598 Western Mediterranean Sea): Marine Geology, v. 275, p. 37–52.

599 Mastbergen, D.R., and Van Den Berg, J.H., 2003, Breaching in fine sands and the generation of
600 sustained turbidity currents in submarine canyons: Breaching in submarine canyons:
601 Sedimentology, v. 50, p. 625–637.

602 Mulder, T., and Alexander, J., 2001, The physical character of subaqueous sedimentary density
603 flows and their deposits: Sedimentology, v. 48, p. 269–299.

604 Mulder, T., and Syvitski, J.P.M., 1995, Turbidity Currents Generated at River Mouths during
605 Exceptional Discharges to the World Oceans: The Journal of Geology, v. 103, p. 285–299.

606 Mulder, T., Savoye, B., and Syvitski, J.P.M., 1997, Numerical modelling of a mid-sized gravity
607 flow: the 1979 Nice turbidity current (dynamics, processes, sediment budget and seafloor impact):
608 Sedimentology, v. 44, p. 305–326.

609 Mulder, T., Savoye, B., Piper, D.J.W., and Syvitski, J.P.M., 1998, The Var submarine
610 sedimentary system: understanding Holocene sediment delivery processes and their importance to
611 the geological record, *in* Stoker, M.S., Evans, D., and Cramp, A. eds., Geological Processes on
612 Continental Margins: Sedimentation, Mass-Wasting and Stability: Geological Society of
613 London, Special Publications129, p. 145–166.

614 Mulder, T., Migeon, S., Savoye, B., and Jouanneau, J.-M., 2001, Twentieth century floods
615 recorded in the deep Mediterranean sediments: Geology, v. 29, p. 1011–1014.

616 Mulder, T., Syvitski, J.P.M., Migeon, S., Faugères, J.-C., and Savoye, B., 2003, Marine
617 hyperpycnal flows: initiation, behavior and related deposits. A review: Marine and Petroleum
618 Geology, v. 20, p. 861–882.

619 Nakajima, T., 2006, Hyperpycnites Deposited 700 km Away from River Mouths in the Central
620 Japan Sea: Journal of Sedimentary Research, v. 76, p. 60–73.

621 Normark, W.R., and Piper, D.J.W., 1991, Initiation processes and flow evolution of turbidity
622 currents: implications for the depositional record, *in* Osborne, R.H. ed., From Shoreline to Abyss:
623 SEPM, Special Publication 46, p. 207-230.

624 Parker, G., Fukushima, Y., and Pantin, H.M., 1986, Self-accelerating turbidity currents: Journal of
625 Fluid Mechanics, v. 171, p. 145-181.

626 Parsons, J.D., Bush, J.W.M., and Syvitski, J.P.M., 2001, Hyperpycnal plume formation from
627 riverine outflows with small sediment concentrations: Sedimentology, v. 48, p. 465–478.

628 Piper, D.J.W., and Savoye, B., 1993, Processes of late Quaternary turbidity current flow and
629 deposition on the Var deep-sea fan, north-west Mediterranean Sea: Sedimentology, v. 40, p. 557–
630 582.

631 Plink-Björklund, P., and Steel, R.J., 2004, Initiation of turbidity currents: outcrop evidence for
632 Eocene hyperpycnal flow turbidites: Sedimentary Geology, v. 165, p. 29–52.

633 Sequeiros, O.E., Naruse, H., Endo, N., Garcia, M.H., and Parker, G., 2009, Experimental study on
634 self-accelerating turbidity currents: Journal of Geophysical Research, v. 114, no. C05025.

635 Shanmugam, G., 2018, The hyperpycnite problem: Journal of Palaeogeography, v. 7, p. 6.

636 Silva Jacinto, R., 2008, SOLVEIG I cruise, L'Europe R/V.

637 Simmons, S.M., Azpiroz-Zabala, M., Cartigny, M.J.B., Clare, M.A., Cooper, C., Parsons, D.R.,
638 Pope, E.L., Sumner, E.J., and Talling, P.J., 2020, Novel Acoustic Method Provides First Detailed
639 Measurements of Sediment Concentration Structure Within Submarine Turbidity Currents:
640 Journal of Geophysical Research: Oceans, v. 125, no. e2019JC015904.

641 Stacey, M.W., and Bowen, A.J., 1988, The vertical structure of turbidity currents and a necessary
642 condition for self-maintenance: Journal of Geophysical Research, v. 93, p. 3543-3553.

643 St-Onge, G., Mulder, T., Piper, D.J.W., Hillaire-Marcel, C., and Stoner, J.S., 2004, Earthquake
644 and flood-induced turbidites in the Saguenay Fjord (Québec): a Holocene paleoseismicity record:
645 Quaternary Science Reviews, v. 23, p. 283–294.

646 Talling, P.J., 2014, On the triggers, resulting flow types and frequencies of subaqueous sediment
647 density flows in different settings: Marine Geology, v. 352, p. 155–182.

648 Talling, P.J., 2021, Fidelity of turbidites as earthquake records: Nature Geoscience, v. 14, p. 113–
649 116.

650 Thorne, P.D., and Hanes, D.M., 2002, A review of acoustic measurement of small-scale sediment
651 processes: Continental Shelf Research, v. 22, p. 603–632.

652 van Loon, A.J., Hüneke, H., and Mulder, T., 2019, The hyperpycnite problem: comment: Journal
653 of Palaeogeography, v. 8, p. 24.

654 Zavala, C., 2019, The new knowledge is written on sedimentary rocks – a comment on
655 Shanmugam's paper "the hyperpycnite problem": Journal of Palaeogeography, v. 8, p. 23.

656 Zavala, C., and Pan, S. X., 2018, Hyperpycnal flows and hyperpycnites: Origin and distinctive
657 characteristics: Lithologic Reservoirs, v. 30, p. 1-27.

658 Zavala, C., Ponce, J.J., Arcuri, M., Drittanti, D., Freije, H., and Asensio, M., 2006, Ancient
659 Lacustrine Hyperpycnites: A Depositional Model from a Case Study in the Rayoso Formation
660 (Cretaceous) of West-Central Argentina: Journal of Sedimentary Research, v. 76, p. 41–59.

661 Zavala, C., Arcuri, M., Di Meglio, M., Gamero, H., and Contreras, C., 2011, A genetic facies tract
662 for the analysis of sustained hyperpycnal flow deposits: American Association of Petroleum
663 Geologists, Studies in Geology, v. 61, p. 31-51.

664

Figure 1. A) Overview map of Var Canyon showing locations of three mooring stations (VH, VE, and VV), and measurement stations for river discharge (Napoleon III) and meteorological data (MeteoFrance). B) Detailed bathymetric maps of each mooring station. Note that mooring VH is offset from the canyon axis, and mooring VV moved a small distance during flows. C) Set-up for each mooring, including both moorings at the VV site. ADCPs measure velocity profiles. RCMs are single-height current meters, and TBD is a turbidity sensor. Height in meters above seafloor (masf) are indicated.

Figure 2. Complete time series of monitoring data. Five turbidity current events are highlighted, and numbered from 1 to 5. The three flows recorded at all moorings are shown by blue boxes, whilst green boxes highlight events only recorded at individual stations. A) Detailed time series of data from land stations. The NapoleonIII station provides river discharge data. Data on wind speed and precipitation come from the MeteoFrance station, and these weather data are normalized using the minimum and maximum values that occurred during the study period. B) Velocity measurements from single-height current meters (RCMs) at station VH, located at 15, 25, and 35 meters above seafloor (masf). C) Velocity measurements from a 300 kHz ADCP at station VE. Maximum velocity, and velocity at 24 masf, are shown for comparison. Particle flux from a sediment trap at station VE, based on a nine-day average. D) RCM velocity measurement from station VV, located at 25 masf, and particle flux based on nine-day average.

Figure 3. Detailed measurements for turbidity current events 1, 4, and 5 (see Fig. 2 for full time series). A) River discharge at the NapeoleonIII station. B) ADCP velocity (maximum recorded and at 25 masf) and temperature data from station VE. C) RCM velocity and temperature data (both at 25 masf) at station VV. The scale is the same for data on velocity and temperature at each station in parts B and C.

691 Figure 4. Comparison of flow structures for the three events recorded at multiple mooring sites
692 (events 1, 4, and 5 in Fig. 2). A) River discharge from Napoleon III station. B) Time-series data from
693 300 kHz ADCP at station VE, showing velocity and sediment concentration (from backscatter
694 inversion) structure of each event. ADCP backscatter inversion is corrected for attenuation, and
695 measurements from the turbidity sensor at 15 masf are shown by blue line, with saturation level
696 indicated by blue dashed line. C) Time-series data from 300 kHz ADCP at station VV, showing
697 velocity and acoustic backscatter structure of each event. At this site, ADCP backscatter data could
698 not be inverted to sediment concentration due to coarse vertical resolution. Red line shows the flow
699 thickness based on calculations of depth-averaged height following Stacey and Bowen (1988).

700

701 Figure 5. Summary figure of how different triggers are linked to subsequent flow structures. A, B)
702 The classic mechanisms pre-existing in literature, showing how specific triggers lead to unique
703 velocity signatures. C, D) Crossover mechanisms discussed in this study. Here, specific triggers do
704 not lead to their expected velocity signatures.

705

Figure1

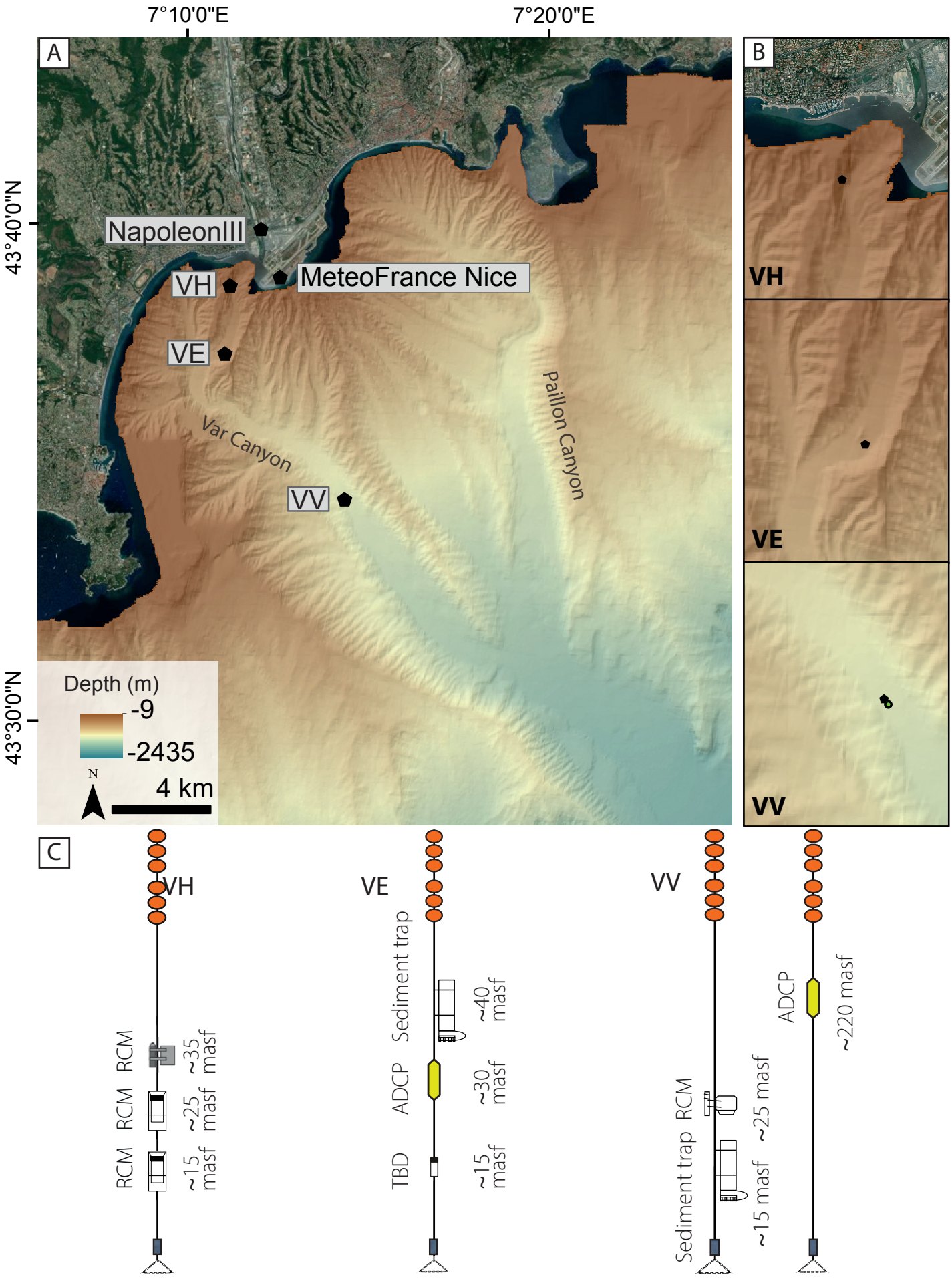
7°10'0"E
7°20'0"E
43°40'0"N
43°30'0"N
A
B
C
NapoleonIII
MeteoFrance Nice
VH
VE
VV
Var Canyon
Paillon Canyon
Depth (m)
-9
-2435
N
4 km
RCM
RCM
RCM
~15 masf
~25 masf
~35 masf
TBD
ADCP
Sediment trap
~15 masf
~30 masf
~40 masf
Sediment trap
RCM
~15 masf
~25 masf
ADCP
~220 masf

Figure2

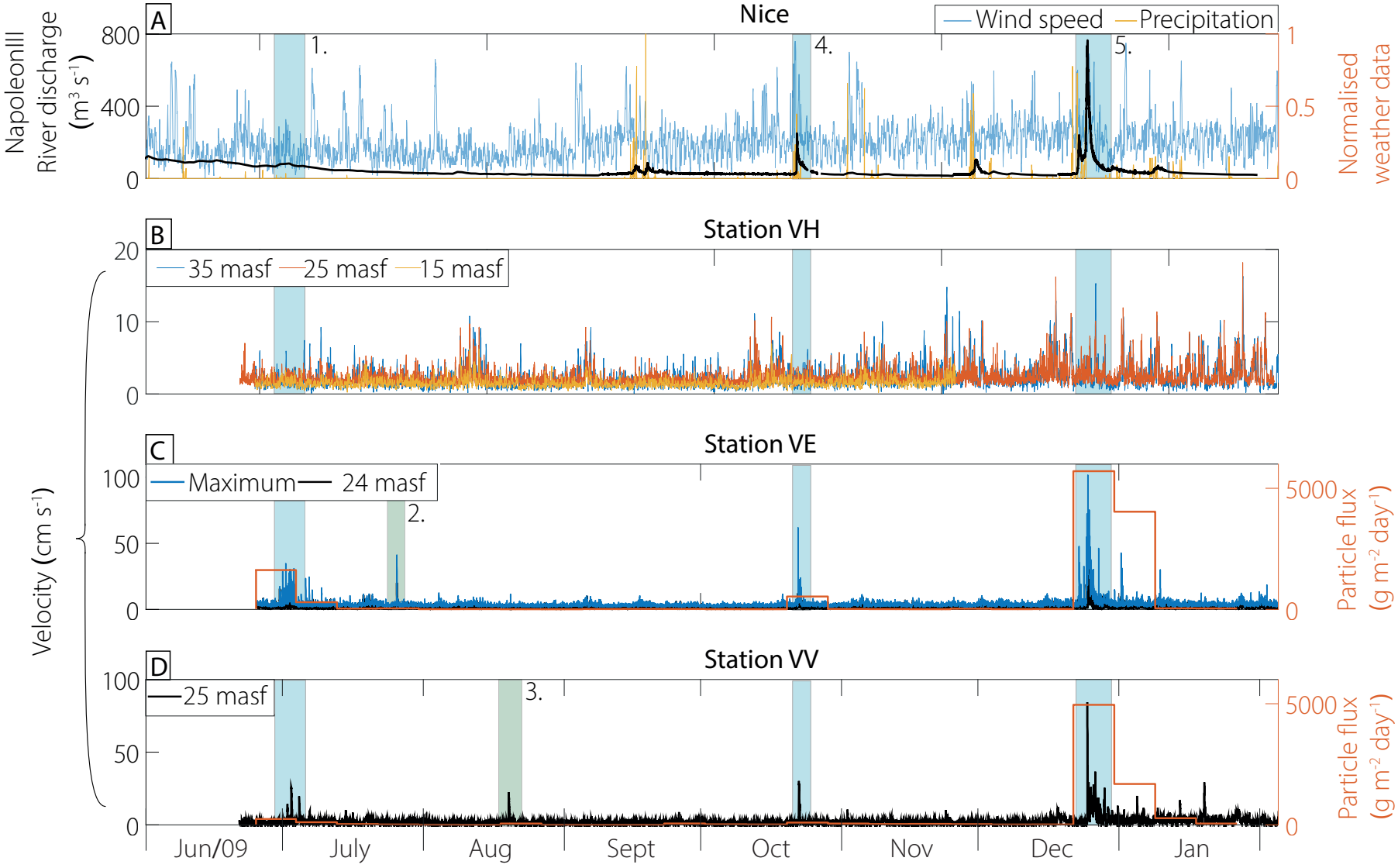
A
Nice
Wind speed
Precipitation
NapoleonIII
River discharge
(m³ s⁻¹)
800
400
0
1.
4.
5.
1
0.5
0
Normalised
weather data
B
Station VH
35 masf
25 masf
15 masf
20
10
0
C
Station VE
Maximum
24 masf
2.
100
50
0
5000
0
Particle flux
(g m⁻² day⁻¹)
Velocity (cm s⁻¹)
D
Station VV
25 masf
3.
100
50
0
5000
0
Particle flux
(g m⁻² day⁻¹)
Jun/09
July
Aug
Sept
Oct
Nov
Dec
Jan

Figure3

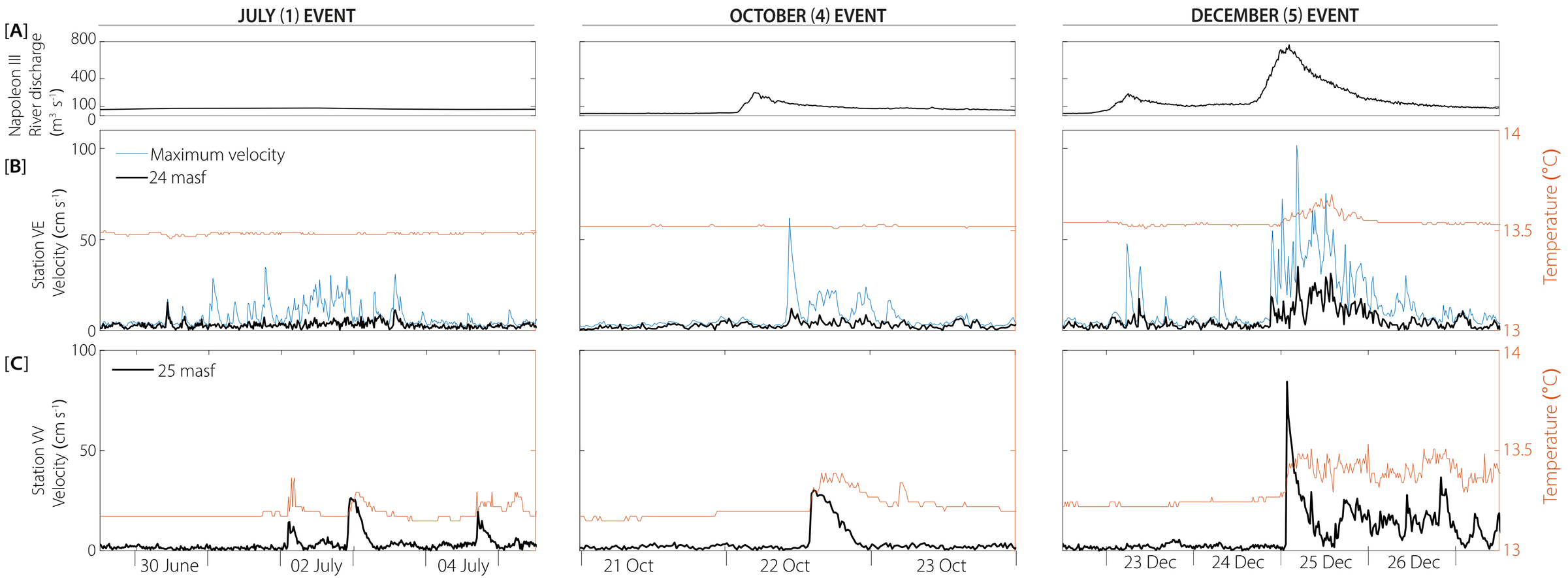
JULY (1) EVENT
OCTOBER (4) EVENT
DECEMBER (5) EVENT
[A]
Napoleon III River discharge (m3 s-1)
800
400
100
0
[B]
Maximum velocity
24 masf
Station VE Velocity (cm s-1)
100
50
0
[C]
25 masf
Station VV Velocity (cm s-1)
100
50
0
Temperature (°C)
14
13.5
13
30 June
02 July
04 July
21 Oct
22 Oct
23 Oct
23 Dec
24 Dec
25 Dec
26 Dec

Figure4

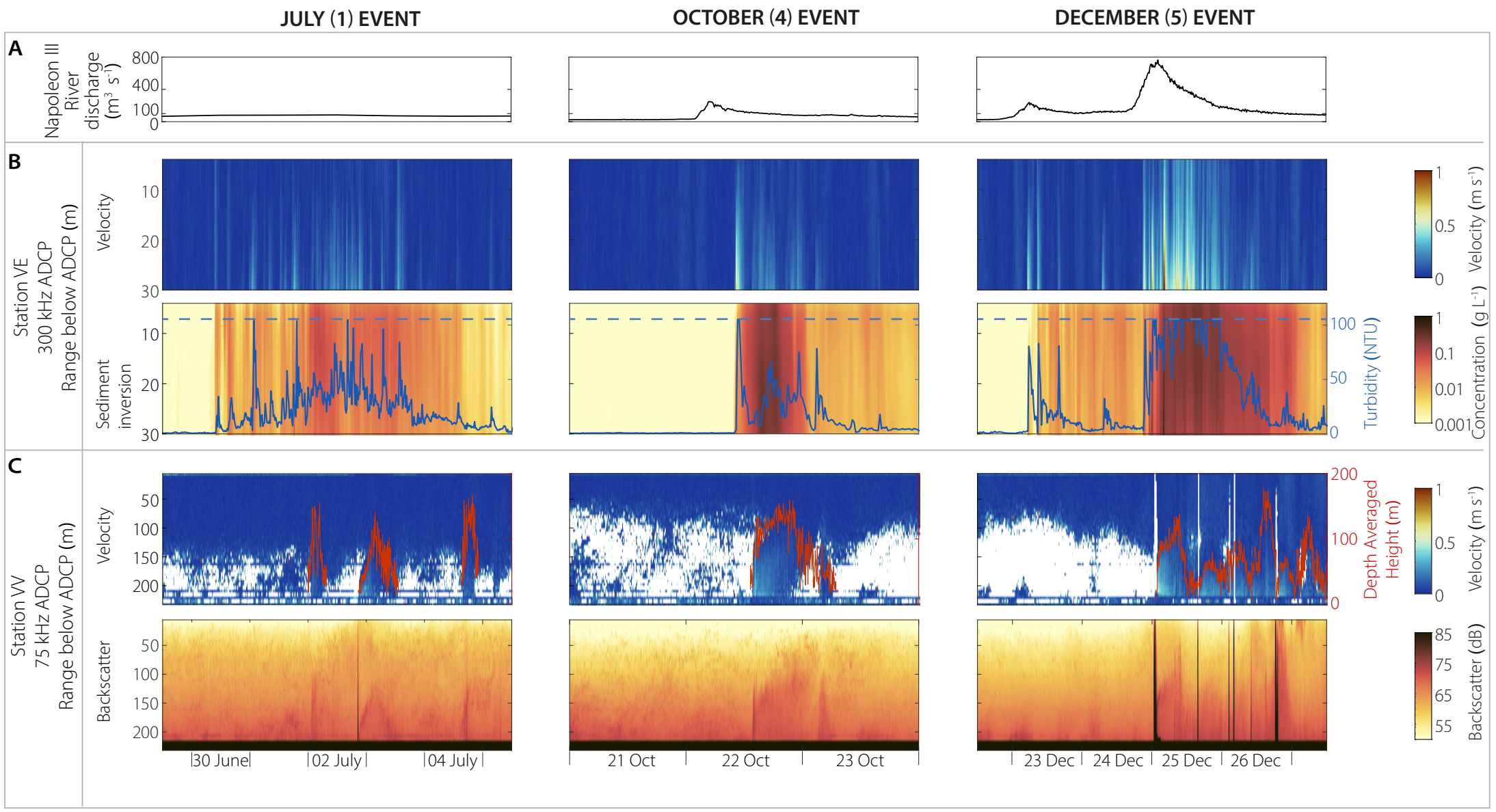
JULY (1) EVENT
OCTOBER (4) EVENT
DECEMBER (5) EVENT
A
Napoleon III River discharge (m³ s⁻¹)
800
400
100
0
B
Station VE
300 kHz ADCP
Range below ADCP (m)
Velocity
Sediment inversion
10
20
30
Turbidity (NTU)
100
50
0
Velocity (m s⁻¹)
1
0.5
0
Concentration (g L⁻¹)
1
0.1
0.01
0.001
C
Station VV
75 kHz ADCP
Range below ADCP (m)
Velocity
Backscatter
50
100
150
200
Depth Averaged Height (m)
200
100
0
Velocity (m s⁻¹)
1
0.5
0
Backscatter (dB)
85
75
65
55
30 June
02 July
04 July
21 Oct
22 Oct
23 Oct
23 Dec
24 Dec
25 Dec
26 Dec

Figure5

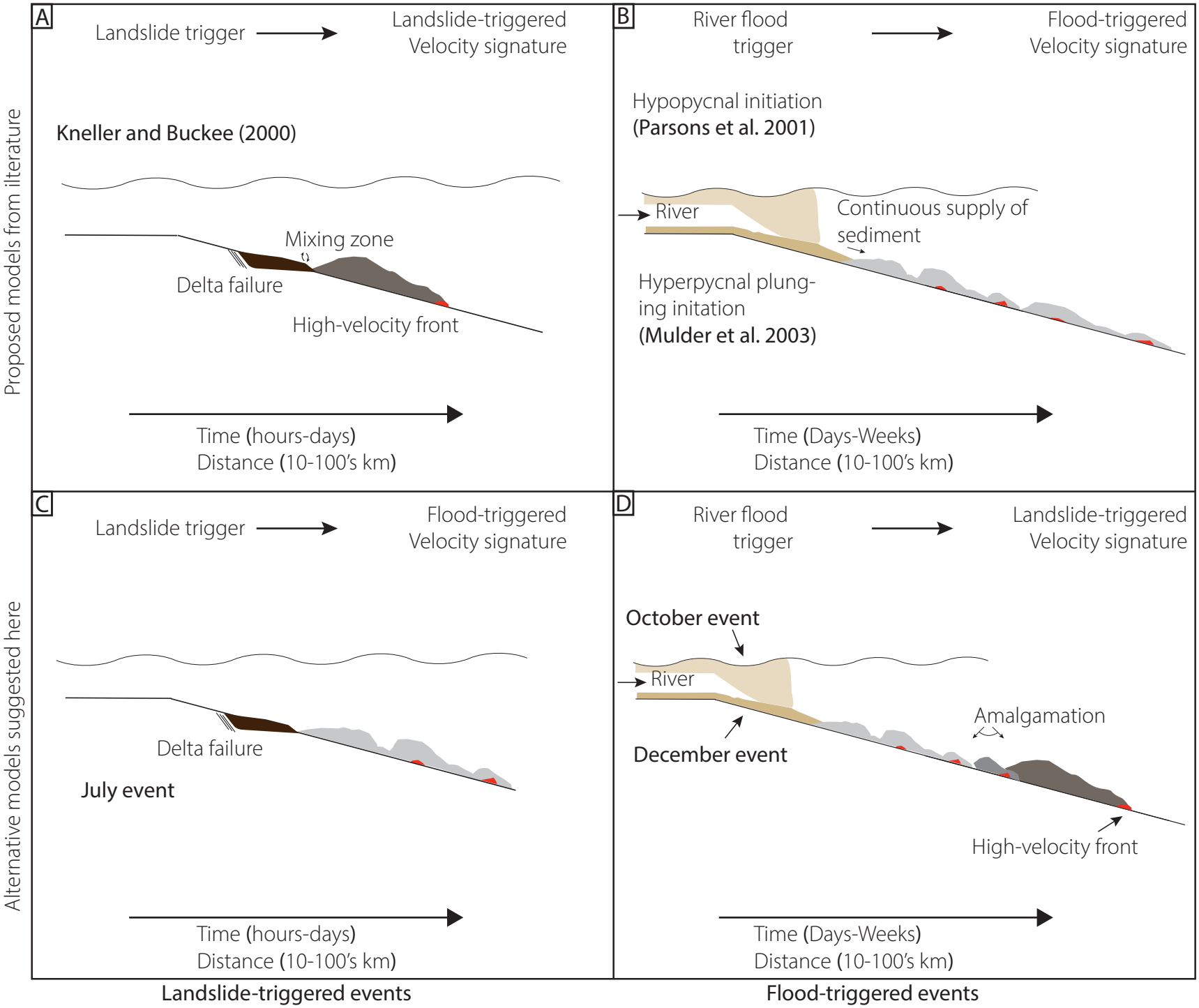
A
Landslide trigger
Landslide-triggered
Velocity signature
Kneller and Buckee (2000)
Mixing zone
Delta failure
High-velocity front
Time (hours-days)
Distance (10-100's km)
B
River flood
trigger
Flood-triggered
Velocity signature
Hypopycnal initiation
(Parsons et al. 2001)
River
Continuous supply of
sediment
Hyperpycnal plung-
ing initation
(Mulder et al. 2003)
Time (Days-Weeks)
Distance (10-100's km)
C
Landslide trigger
Flood-triggered
Velocity signature
Delta failure
July event
Time (hours-days)
Distance (10-100's km)
D
River flood
trigger
Landslide-triggered
Velocity signature
October event
River
Amalgamation
December event
High-velocity front
Time (Days-Weeks)
Distance (10-100's km)
Proposed models from literature
Alternative models suggested here
Landslide-triggered events
Flood-triggered events

Table1

Table 1. Overview of three main events measured at multiple sites (events 1, 4, and 5 in Fig. 3).

		JULY [Event 1]		OCTOBER [Event 4]		DECEMBER [Event 5]*	
Var River	**River discharge (m^3/s)**	80		250		765	
	Calculated Suspended Sediment Concentration (kg/m^3) (after Mulder et al. 1998)	0.2-3		4-8		20-50	
Var Canyon	**Station**	**VE**	**VV**	**VE**	**VV**	**VE**	**VV**
	Onset	Gradual	Sudden	Sudden	Sudden	Sudden	Sudden
	Cycles of velocity	Multiple surges	3 distinct repeats	Multiple surges	1 acceleration	Multiple cycles	1 acceleration
	Peak velocity (cm/s) [transit velocity]	34.8	26.4 [6.9]	61.8	30.2 [75.8]	101.6	84.4 [64.1]
	Flow duration (hrs)	79-81 hrs	71-78 hrs	21-25 hrs	10-13 hrs	39-41 hrs	85-97 hrs
	Flow height (m) [approx]	~20 m	150 m	> 30 m	130 m	> 30 m	150 m
	Temperature rise (° Celsius)	0	0.2	0	0.2	0.2	0.2
	Sediment flux ($g/m^2/day$)	1624	242	532	90	5707	4956

*Only second stage of December event, 25th December onwards